
NUMERICAL SIMULATION OF THE PILE INTEGRITY TEST ON DEFECTED PILES

MLADEN ĆOSIĆ, BORIS FOLIĆ AND RADOMIR FOLIĆ

about the authors

Mladen Ćosić
University of Belgrade,
Faculty of Civil Engineering
Marka Milanovića 17, 15300 Loznica, Serbia
E-mail: mladen.cosic@ymail.com

Boris Folić
University of Belgrade,
Faculty of Mechanical Engineering
E-mail: boris.folic@gmail.com

Radomir Folić
University of Novi Sad,
Faculty of Technical Sciences
E-mail: folic@uns.ac.rs

abstract

This paper deals with the development of a discrete numerical 2D and 3D solid pile model with a discontinuity and defects to simulate non-destructive testing using the pile integrity test (PIT). The pile discontinuity and defects were modelled by reducing the specific finite elements and the elastic modulus of concrete. The wave-propagation response of the pile was analyzed based on a step-by-step numerical integration using the Hilber-Hughes-Taylor (HHT) method in the time domain. The concept of a system-response analysis was originally formulated based on the integration of individual reflectograms into a reflectogram surface, which is generated in a 3D cylindrical coordinate system. The use of reflectogram surfaces enables an understanding of wave propagation based on their velocity to a higher level than is usually the case with standard, one-dimensional reflectograms. Changes in the velocity responses on the reflectogram, shifting from a positive to a negative value, point to the locations of discontinuities and defects in the discrete 3D pile model, and there is a clear difference in the reflectograms, depending on the position of the measuring point. The study defines the typological models of the reflectogram: without discontinuities and defects, pile-head defect, defect in the middle of the pile length or a reduced modulus of elasticity in the middle of the pile length, pile-base defect or reduced modulus of elasticity in the pile-base zone and reduced modulus of elasticity in the pile-head zone.

keywords

reflectogram surface, numerical pile model, solid finite elements

1 INTRODUCTION

Dynamic non-destructive testing (NDT) methods are usually accompanied by low stress and strain states in the pile in the linear-elastic behaviour of a material. The pile integrity test (PIT) is a fast and reliable method, mostly used for evaluating the condition of the pile in the soil. It is based on the reflection of the waves emitted from the pile head towards the pile toe. The quality and integrity of the placed pile is identified by verifying the actual length and diameter of the pile, its discontinuities, defects and damages. However, despite the proven reliability of the PIT test, there are a number of issues regarding this method, such as the effect of the propagation of the emitted waves through the pile at different levels and models of the discontinuities and defects. In [1] the authors describe a special method for monitoring the dynamic pile-testing sensors, based on strain tensors, installed inside the pile body. The results of the measured experimental investigation are compared with a numerical study of the pile and soil model in the software PLAXIS. The specific aspects of measuring the strains of the pile in the interaction with the ground for dynamic testing, where the sensors are fixed to the expansion-reinforcing bars, are shown in the paper too [2]. In addition to testing the piles in real conditions using the PIT test, tests can be conducted based on simulating analytical and numerical methods, such as the finite-element method (FEM). In [3], the numerical modelling of a tube system pile is discussed using 3D solid finite elements, while the pile defects were simulated with a series of PIT tests based on changes in the pile-wall thickness and in the Young's elastic modulus. A numerical analysis using the PIT simulation and the wave propagation through the pile and the soil is described in [4] and [5] using the CEFIT software.

The pile integrity using the PIT simulation and artificial neural networks (ANNs) was tested in [6]. Unlike the aforementioned studies, paper [7] describes the numerical aspects of resolving the wave equation for a pile using the MAPLE, ANSYS and WEAP 87 software.

This paper summarizes the theoretical basis for the treatment of wave propagation in piles with and without a discontinuity when using the PIT. The defects were identified based on processing the reflectograms that were subsequently integrated into a single response using the reflectogram surface, originally introduced in this study. The discontinuity and defects in the pile were modelled using a NDT simulation and 3D solid finite elements. This allowed the defects in the pile to be presented in a more detailed manner by eliminating some of the solid finite elements. The aspects of wave propagation in the pile were considered for various angles of impacts, while specific solutions were subsequently processed and integrated into the 3D response model.

2 TREATING WAVE PROPAGATION IN THE PILE USING THE PIT

The PIT is based on the principle of the induction, propagation, reflection, refraction and reception of waves in the pile. Waves, as external excitation, are caused by using a striking hammer. Upon the initiation, the wave expands (propagates) through the pile from its head towards the toe and vice versa. The effect of reflection occurs at the interface of two different media – in this case, at the pile toe-soil surface where the wave propagates towards the pile head. If the wavelength is longer than or equal to the pile diameter, then the wave propagation through the pile may be considered using the one-dimensional wave-propagation theory in a solid medium [8]. The one-dimensional wave equation (along the x) is:

$$\frac{\partial^2 u}{\partial t^2} = v^2 \frac{\partial^2 u}{\partial x^2}, \quad (1)$$

while the general solution of this equation is as follows:

$$u(t) = u_1(x - vt) + u_2(x + vt). \quad (2)$$

where v is the wave velocity, u is displacement, and t is time. The velocity of propagation of longitudinal waves in a solid medium v is a function of the given medium's material properties and is determined by:

$$v = \sqrt{\frac{E}{\rho}} \quad \text{or} \quad v = \sqrt{\frac{E(1-\mu)}{\rho(1+\mu)(1-2\mu)}}, \quad (3)$$

where E is the Young's modulus, ρ is the bulk weight, and μ is the Poisson's ratio. For simpler systems and contour conditions, the solution for Equations (1) can be obtained in a closed form; however, more complex pile models with discontinuities and defects require the use of the finite-element method.

The dynamic load applied to the pile head is a sinus function, while only half of the sine wave is taken into consideration [9]:

$$p = p_0 \sin \omega t \quad \text{for} \quad 0 \leq t \leq \frac{T}{2}, \quad (4)$$

where T is the vibration period of the external excitation. The expression that defines the relationship between the wavelength λ , the wave-propagation velocity v and the frequency f is as follows:

$$\lambda = \frac{v}{f}. \quad (5)$$

The time t required for the wave to travel through the pile is measured from the moment of initiation by an external excitation, throughout its propagation through the pile, reflection at the toe and its return to the pile head. Changes in the wave propagation through the pile over time are displayed in a reflectogram (reflect signal). The pile length L is determined, based on the reflectogram, according to [10]:

$$L = \frac{vt}{2}. \quad (6)$$

The wave-propagation velocity through the pile is estimated using an accelerometer. The resulting accelerogram is then further corrected (amplified and filtered), integrated and presented over the change in the wave-propagation velocity through the pile. The pile length in the soil is determined for a time interval $[t_1, t_2]$, where the initiation of waves in the pile head corresponds with the peak velocity v_1 , while the reflected wave in the pile head corresponds with the peak velocity v_2 .

The shape of the reflectogram is significantly influenced by the material properties of the pile, and also influenced by the effects of wave reflection and refraction at the pile-soil interface. Depending on the soil strength, and the quality and type in the pile-toe zone, the reflected signal can have either a positive or a negative value. If the soil in the pile-toe base is very stiff, then the reflected signal is negative; if the stiffness of this soil is low, then the reflected signal is positive [11]. Due to the friction that occurs at the pile mantle-soil interface, the reflected wave can be of a smaller magnitude, resulting in problems with the interpretation of the reflectogram in the case of extremely long piles.

3 TREATING WAVE PROPAGATION IN A PILE WITH DISCONTINUITIES

A pile-integrity analysis is based on the one-dimensional wave-propagation theory. Wave reflection, generated by the impedance Z changing (discontinuity), extends all the way to the pile head, where the reflectogram records these changes. The changes in the reflectogram generally occur due to changes in the pile toe, changes in the pile diameter along its mantle, as a result of a partial inclusion of the soil into the pile, cracks, due to variation in the quality of pile material and/or soil layers, and the influence of reinforcing steel in the pile (in the case of a strongly reinforced pile).

The possible variations in the response to the propagation of waves along the pile discontinuity on the reflectogram are implied by the appearance of a positive or negative wave. The existence of discontinuities and defects in the pile is reflected through changes in the velocity on the reflectogram, where the following cases are possible: “normal” pile length without discontinuities and defects (Figure 1a), problem with the pile head (Figure 1b), discontinuity or impedance reduction (Figure 1c), the pile length is shorter than designed (Figure 1d), the pile length is longer than designed (Figure 1e) and there is a deviation or there is a lack of clear wave reflection in the pile toe (Figure 1f). The option for determining the quality of a given reflectogram is to record the signal for a number of measuring points, or enter the pulse at some other suitable location on the pile head.

4 PROCESSING THE REFLECTOGRAM SIGNALS

Reflectogram signals are processed in order to facilitate the adjustment, presentation and interpretation of the recorded values. The processing procedures are conducted in accordance with the signal theory, i.e., amplification, filtering and analysis of Fourier of transforms. The procedure of amplification involves the amplification of either the entire reflectogram or only a part of it, based on traditional scaling or advanced techniques: linear or exponential [10]. This procedure is especially useful when amplification on the recorded reflectogram cannot be clearly identified or the magnitude of the reflected wave is reduced. If a number of minor discontinuities or defects exist along the pile, then the reflectogram contains frequency oscillations in amplitudes of discrete velocity values, which makes it difficult to determine the actual pile length, and requires filtering.

In order to minimize the filtering error, the iterative filtering technique is used, where the reflectogram peaks are gradually reduced. It is particularly useful to apply a low-pass filter that eliminates the span of higher frequencies [12]. In the low-pass filter it is possible to apply a Butterworth function that describes the principle of conservation and elimination of frequencies, while their construction is based on the transfer function. The frequency domain analysis (FDA) of the reflectogram is based on the use of the discrete Fourier transformation (DFT) [13]:

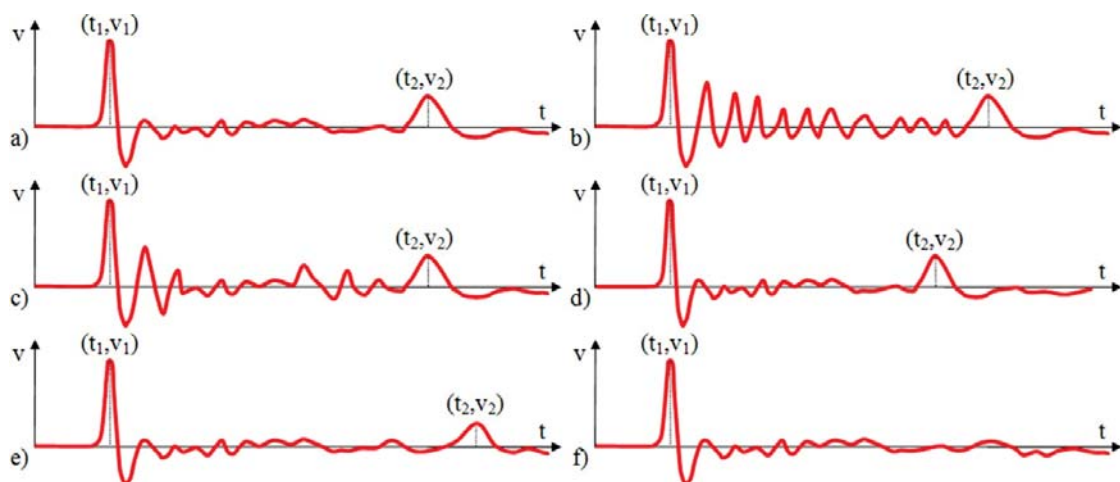


Figure 1. Reflectograms: a) “normal” pile length without discontinuities and defects, b) problem with the pile head, c) discontinuity in impedance reduction, d) pile length is shorter than designed, e) pile length is longer than designed, f) there is a deviation or there is a lack of clear wave reflection in the pile toe.

$$G(n) = \frac{1}{N} \sum_{k=0}^{N-1} g(k) e^{-\frac{2\pi jkn}{N}} \quad \text{for } n = 0, \dots, N-1, \quad (7)$$

$$g(n) = \sum_{k=0}^{N-1} G(k) e^{\frac{2\pi jkn}{N}} \quad \text{for } n = 0, \dots, N-1. \quad (8)$$

The frequency response realized through the Fourier transformation is presented through the Fourier amplitude spectrum (FAS):

$$\text{amp} = \sqrt{\text{Re}(G(f))^2 + \text{Im}(G(f))^2}. \quad (9)$$

5 NUMERICAL MODELLING AND ANALYSIS OF THE DISCONTINUITIES AND DEFECTS IN THE PILE

Modelling the pile and analyzing the wave propagation using the PIT simulation test can be carried out in the following ways: using the analytical method to a lumped mass model (LMM), method of characteristics (MC), finite-difference method (FDM) and the finite-element method (FEM). Using the finite-element method enables the PIT simulation test for the 1D discrete pile model with the 2D or 3D discrete soil model; for the 2D discrete pile model with the 2D discrete soil model; and for the 3D discrete pile model with the 3D discrete soil model. The above-presented options are for explicit soil modelling by using the 2D or 3D discrete model; however, it is also possible to be taken implicitly into the soil-pile interaction analysis. The present study is based on the simulation of PIT of the 3D discrete homogeneous and inhomogeneous elastic pile model with the implicitly implemented effects of pile-soil interaction. The components of soil stiffness were introduced over replacement springs, while the damping was introduced through the damping elements according to [14]:

$$k_v = 2.3G_s, c_v = 2\pi\rho_s V_s d, K_v = \frac{4G_s d}{1-\mu_s}, C_v = \frac{0.85K_v d}{V_s}, \quad (10)$$

where k_v is the vertical stiffness component for the pile mantle, c_v is the vertical damping component for the pile mantle, K_v is the vertical stiffness component for the pile toe, C_v is the vertical damping component for the pile toe, ρ_s is soil bulk density, d is the pile diameter, μ_s is the Poisson's ratio of the soil, and V_s is the shear wave propagation velocity:

$$V_s = \sqrt{\frac{G_s}{\rho_s}}, \quad (11)$$

where G_s is the shear modulus of the soil:

$$G_s = \frac{E_s}{2(1+\mu_s)}, \quad (12)$$

and E is Young's elastic modulus for the soil.

The process of determining the acceleration, velocity and displacement of the pile using the PIT is based on considering the differential equations of motion:

$$[M]\{U\} + [C]\{V\} + [K]\{D\} = \{Q\}, \quad (13)$$

where $[M]$ is the mass matrix, $\{U\}$ is the acceleration vector, $[C]$ is the damping matrix, $\{V\}$ is the velocity vector, $[K]$ is the stiffness matrix, $\{D\}$ is the displacement vector and $\{Q\}$ is the vector of external loads. The Equations (13) are resolved using step-by-step numerical integration with a modified form of the Hilber-Hughes-Taylor (HHT) method [15]:

$$[M]\{U\}_{i+1} + (1+\alpha)[C]\{V\}_{i+1} - \alpha[C]\{V\}_i + (1+\alpha)[K]\{D\}_{i+1} - \alpha[K]\{D\}_i = \{Q\}_{i+\alpha}, \quad (14)$$

and for a moment of time:

$$t_{i+1} = t_i + \Delta t. \quad (15)$$

In order to achieve a high-quality numerical solution for wave propagation both in the discrete numerical model and in the actual soil model, the length of one side of the finite element Δl needs to be [16]:

$$\Delta l = \frac{\lambda}{10}. \quad (16)$$

Numerical modelling of the pile degradation is carried out by analyzing the pile using the staged degradation analysis (SDA). The SDA is constructed so that the pile degradation is generated and simulated by linking the individual analyses. These analyses are successively implemented using the system stiffness matrix from the end of the previous analysis of the degraded condition as the initial system stiffness matrix of the next analysis of degradation. The mathematical formulation of the SDA is derived by starting from the expression for the condition before testing the pile using the PIT:

$$t = 0: [K_0]\{U_0\} = \{P_0\}, \quad (17)$$

where $[K_0]$ is the non-degraded pile stiffness matrix. For the initial stage of pile degradation, the analysis is as follows:

$$t = 1: [K_1]\{U_1\} = \{P_1\}, \quad [K_1] = [K_0] - [K'_0], \quad (18)$$

$$[M_1] = [M_0] + [M'_1],$$

where $[K'_0]$ is the stiffness matrix of the eliminated domain of finite pile elements, $[M_0]$ is the non-degraded pile mass matrix, $[M'_1]$ is the mass matrix of the eliminated domain of finite pile elements. In the i -th stage of pile degradation, the analysis is conducted according to:

$$t = i: [K_i]\{U_i\} = \{P_i\}, [K_i] = [K_{i-1}] - [K'_{i-1}], \\ [M_i] = [M_{i-1}] + [M'_i], \quad (19)$$

while for the n -th stage the following applies:

$$t = n: [K_n]\{U_n\} = \{P_n\}, [K_n] = [K_{n-1}] - [K'_{n-1}], \\ [M_n] = [M_{n-1}] + [M'_n], \quad (20)$$

where $[K_n]$ is the pile stiffness matrix in the final stage of degradation, and $[M_n]$ is the pile mass matrix in the final stage of degradation.

6 DISCUSSION OF THE RESULTS OF NUMERICAL TESTING OF THE PILE DISCONTINUITIES AND DEFECTS

The numerical simulation of the non-destructive pile testing was carried out by using the SAP 2000 software [17]. Before processing the 3D model of the pile with defects, numerical analyses were carried out on a 2D pile and soil model, with each model using more than 40000 surface finite elements. Only part of the finite-element mesh for each model has been shown separately. Figure 2 shows the 2D numerical pile and soil models: model 1 - no discontinuities and defects (Figure 2a), model 2 - pile head defect (Figure 2b), model 3 - defect in the

middle of the pile length (Figure 2c), model 4 - pile base (toe) defect (Figure 2d), model 5 - reduced modulus of elasticity in the pile-head zone (Figure 2e), model 6 - reduced modulus of elasticity in the mid of the pile length (Figure 2f) and model 7 - reduced modulus of elasticity in the pile base (toe) (Figure 2g). The dimensions of the pile considered in the study were $L=15\text{m}$ and $d=0.5\text{m}$; regarding the quality of materials: concrete bulk mass $\rho=2400\text{kg/m}^3$, Young's elastic modulus of concrete $E=30\text{GPa}$, Poisson's ratio of concrete $\mu=0.2$, and the corresponding velocity of wave propagation in concrete $v=3535.53\text{m/s}$. The external impulsive load applied to the pile head is $Q=1\text{KN}$, while the sine wave oscillation period is $T=1\text{ms}$, the corresponding oscillation frequency $f=1\text{kHz}$ and the wavelength $\lambda=3.73\text{m}$. The expected wave-propagation time through the pile is $t=8.2\text{ms}$. In the HHT procedure a time increment of $\Delta t=0.01\text{ms}$ was used, while the total number of steps in the analysis was 1200, so that the considered time interval of the reflectogram is 12ms. All the reflectograms were filtered using a low-pass filter and a weighted-average smoothing filter to obtain a smooth response function for facilitating the interpretation of results, while avoiding the elimination of important peaks. Additionally, spline interpolation was applied to the discrete values of the reflectogram.

A parametric analysis was conducted in order to consider the impact of the changes in the modulus of elasticity of soil below the pile base and around the pile on the shape of the reflectogram. Figure 3 shows the resulting reflectograms for: model 1 - no discontinuities and defects while changing the modulus of elasticity of the soil below the pile base (Figure 3a), model 1 - no discontinuities and defects while changing the modulus of elasticity of the soil around the pile (Figure 3b),

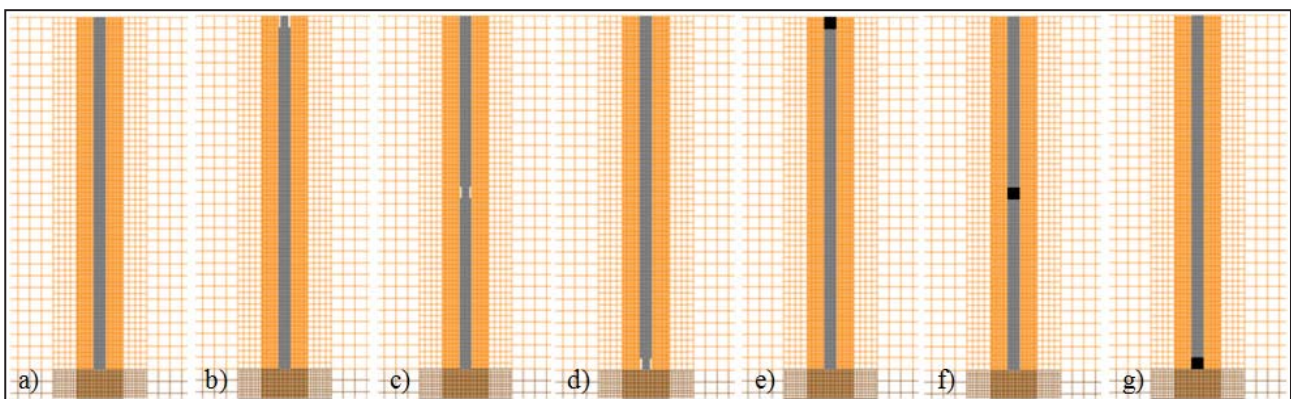


Figure 2. Numerical pile models: a) model 1 - no discontinuities and defects, b) model 2 - pile-head defect, c) model 3 - defect in the middle of the pile length, d) model 4 - pile-base (toe) defect, e) model 5 - reduced modulus of elasticity in the pile-head zone, f) model 6 - reduced modulus of elasticity in the middle of the pile length, g) model 7 - reduced modulus of elasticity in the pile base (toe).

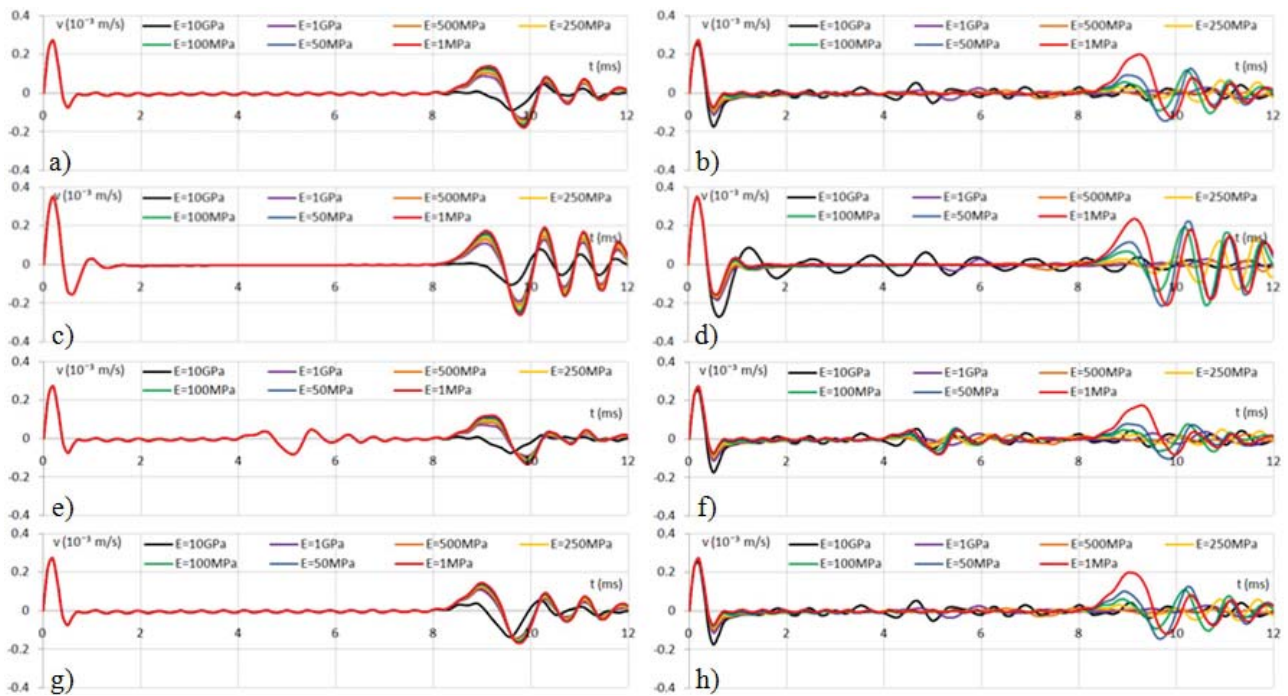


Figure 3. Reflectograms: a) model 1 - no discontinuities and defects while changing the modulus of elasticity of the soil below the pile base, b) model 1 - no discontinuities and defects while changing the modulus of elasticity of the soil around the pile, c) model 2 - pile-head defect while changing the modulus of elasticity of the soil around the pile, d) model 2 - pile-head defect while changing the modulus of elasticity of soil below the pile base, e) model 3 - defect in the middle of the pile length while changing the modulus of elasticity of the soil below the pile base, f) model 3 - defect in the middle of the pile length while changing the modulus of elasticity of the soil around the pile, g) model 4 - pile base (toe) defect while changing the modulus of elasticity of the soil below the pile base and h) model 4 - pile base (toe) defect while changing the modulus of elasticity of the soil around the pile.

model 2 - pile head defect while changing the modulus of elasticity of the soil below the pile base (Figure 3c), model 2 - pile head defect while changing the modulus of elasticity of the soil around the pile (Figure 3d), model 3 - defect in the middle of the pile length while changing the modulus of elasticity of the soil below the pile base (Figure 3e), model 3 - defect in the middle of the pile length while changing the modulus of elasticity of the soil around the pile (Figure 3f), model 4 - pile base (toe) defect while changing the modulus of elasticity of the soil below the pile base (Figure 3g) and model 4 - pile base (toe) defect while changing the modulus of elasticity of the soil around the pile (Figure 3h). Comparing the resulting reflectograms, the locations of the changes in the signal are clearly identified and they correspond to the position of the pile defects. In the case of the defect in the pile head, both positive and negative velocity values are increased in the defect area; the period of oscillation is also increased. In the case of the defect in the middle of the pile length, the signal shifts from a positive to a negative value, clearly indicating the position of the pile defect, while in the case of

the pile base defect, the signal shifts its velocity value somewhat earlier. Changes in the modulus of elasticity of the soil below the pile base do not induce changes in the reflectogram, except in cases of very high values of the modulus of elasticity; in these cases the velocities are reduced. Changes in the modulus of elasticity of the soil around the pile influence the shape of reflectogram to a greater degree than the changes in the modulus of elasticity of the soil below the pile base. In this case, when increasing the modulus of elasticity of the soil, and in particular at very high values of the elastic modulus, the velocity values begin to oscillate slightly at about the value of zero. However, the times for the initiation of defects in the pile are not significantly changed, which can be seen in the reflectogram for the defect in the middle of the pile length.

Figure 4 shows the resulting reflectogram for: model 1 - no discontinuities and defects while changing the modulus of elasticity of the soil below the pile base (Figure 4a), model 1 - no discontinuities and defects while changing the modulus of elasticity of the soil

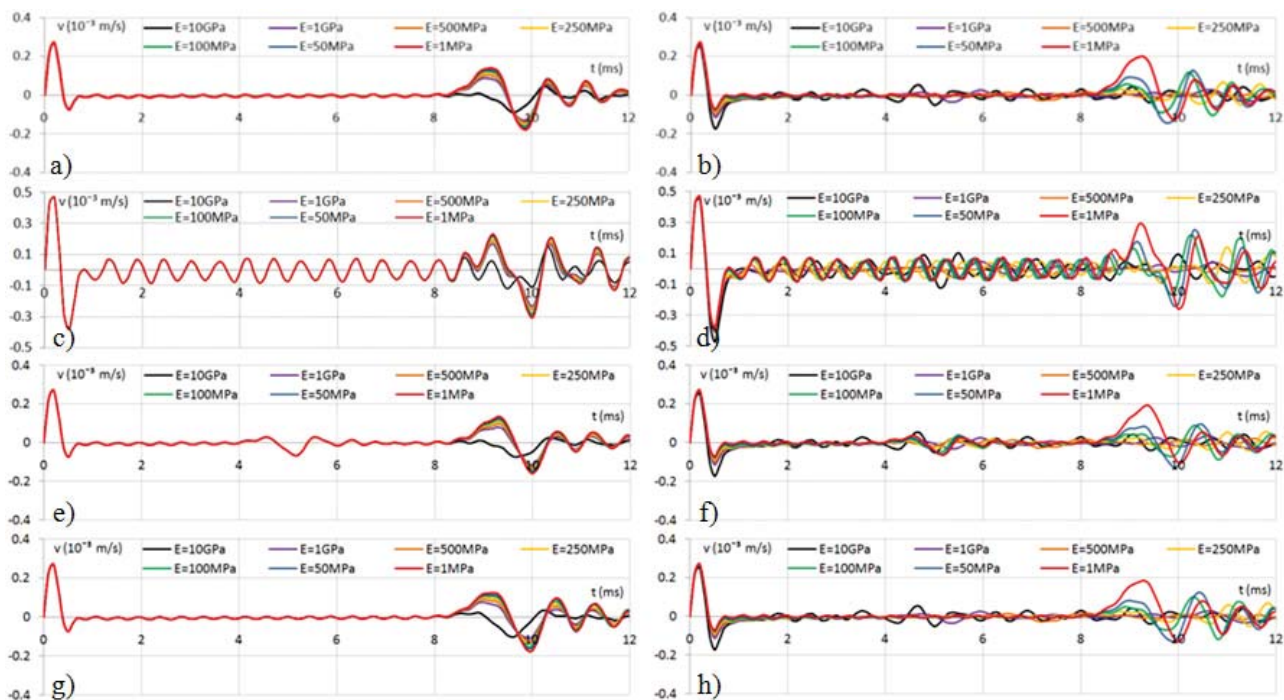


Figure 4. Reflectograms: a) model 1 - no discontinuities and defects pile base (toe) defect while changing the modulus of elasticity of the soil below the pile base, b) model 1 - no discontinuities and defects pile base (toe) defect while changing the modulus of elasticity of the soil around the pile, c) model 2 - reduced modulus of elasticity in the area in the pile-head zone while changing the modulus of elasticity of the soil below the pile base, d) model 2 - reduced modulus of elasticity in the pile head zone while changing the modulus of elasticity of the soil around the pile, e) model 3 - reduced modulus of elasticity in the middle of the pile length while changing the modulus of elasticity of the soil below the pile base, f) model 3 - reduced modulus of elasticity in the middle of the pile length while changing the modulus of elasticity of the soil around the pile, g) model 4 - reduced modulus of elasticity in the pile base (toe) zone while changing the modulus of elasticity of the soil below the pile base and h) model 4 - reduced modulus of elasticity in the pile base (toe) zone while changing the modulus of elasticity of the soil around the pile.

around the pile (Figure 4b), model 2 - reduced modulus of elasticity in the pile-head zone while changing the modulus of elasticity of the soil below the pile base (Figure 4c), model 2 - reduced modulus of elasticity in the pile-head zone while changing the modulus of elasticity of the soil around the pile (Figure 4d), model 3 - reduced modulus of elasticity in the middle of the pile length while changing the modulus of elasticity of the soil below the pile base (Figure 4e), model 3 - reduced modulus of elasticity in the middle of the pile length while changing the modulus of elasticity of the soil around the pile (Figure 4f), model 4 - reduced modulus of elasticity in the pile base (toe) while changing the modulus of elasticity of the soil below the pile base (Figure 4g) and model 4 - reduced modulus of elasticity in the pile base (toe) zone while changing the modulus of elasticity of the soil around the pile (Figure 4h). As in the previous case, comparing the resulting reflectograms the locations of changes in the signal are identified, and they correspond to the positions of the reduction in the modulus of elasticity of the pile. In the case of a

reduction in the modulus of elasticity of the pile head, both the positive and negative velocity values are now much more increased in this area, and the period of oscillation is also increased. This results from the fact that the zone of reduction of the modulus of elasticity of concrete comprises the entire cross-section, while for the simulation of the pile defect only the cross-sectional area has been reduced. Upon the initiation of the reduction of the modulus of elasticity of the pile head, the reflectogram indicates changes in the velocity similar to a sinusoidal function. However, despite the differences in the middle of the reflectogram of the healthy pile and the pile with a reduced modulus of elasticity in its head, the time of transition of the waves from the pile base to the soil below the pile can be clearly observed. In the case of a defect in the middle of the pile length, similar to the previous case, the signal shifts from a positive to a negative value, clearly indicating the position of the pile defect, while in case of the pile base defect, the signal shifts its velocity value somewhat earlier. Changes in the modulus of elasticity of the soil below the pile base do

not induce changes in the reflectogram, except in cases of very high values of the modulus of elasticity; in these cases the velocities are being reduced when the waves cross the zone between the pile base and the soil below the pile. Changes in the modulus of elasticity of the soil around the pile influence the shape of reflectogram to a greater degree than changes in the modulus of elasticity of the soil below the pile base. In this case, when increasing the modulus of elasticity of the soil, and in particular at very high values of the elastic modulus, the velocity values also begin to oscillate slightly at about a zero value for the reduced modulus of elasticity in the middle of the pile length and in the pile base zone.

Figure 5a shows the 3D pile model as generated from 3D solid finite elements, Figure 5b shows a segment of the pile cross-section. Figure 5c shows the sensor locations (positions for which the reflected waves were measured) and the central position for applying the impact loading. The values of the stiffness components are $k_v=10^2\text{N/m}^3$ and $K_v=10^5\text{N/m}^3$, and the values of the damping components are $c_v=10\text{Ns/m}^3$ and $C_v=10^4\text{Ns/m}^3$. Numerical modelling was considered for the model without defects and discontinuities and for seven models with varying pile discontinuities and defects: model 1 - no discontinuities and defects (Figure 6a), model 2 - asymmetric pile toe defect (elimination of specific finite elements

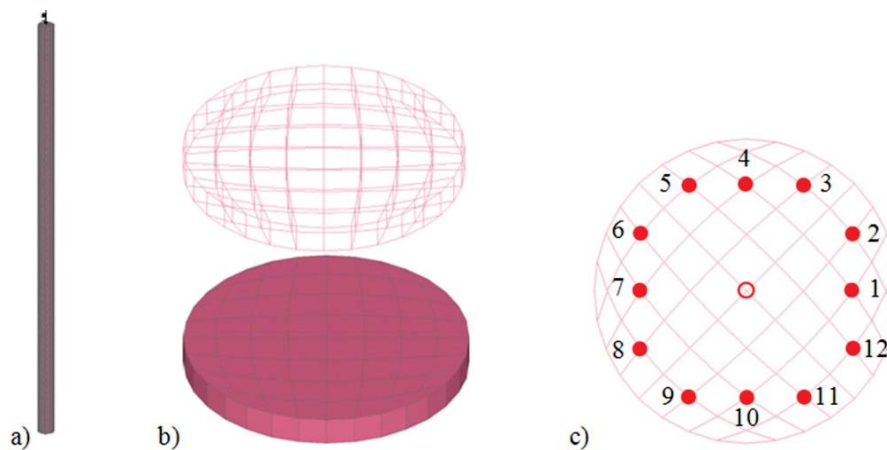


Figure 5. a) the 3D pile model generated from 3D solid finite elements, b) a pile segment, c) sensor locations (positions for which the reflected waves were measured) and the central position of applying the impact loading.

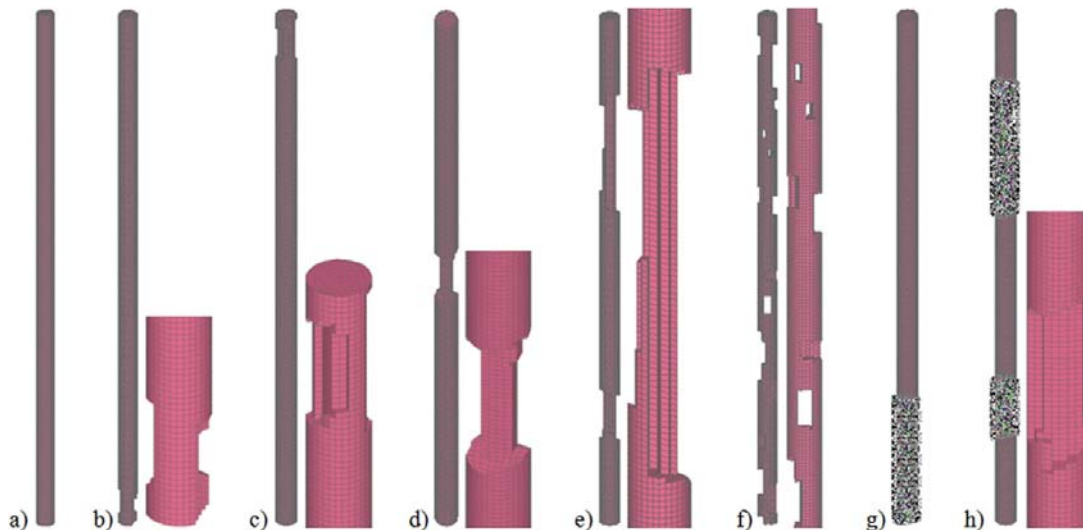


Figure 6. Numerical pile models: a) model 1 - without discontinuities and defects, b) model 2 - asymmetric pile-toe defect, c) model 3 - asymmetric pile-head defect, d) model 4 - asymmetric reduction of cross-section in the middle of the pile length, e) model 5 - asymmetric reduction of cross-section in two locations along the pile length, f) model 6 - significantly degraded pile along its full length, g) model 7 - different elastic modulus in pile-toe zone, h) model 8 - different elastic modulus and asymmetric reduction of cross-section in two locations along the pile.

in a length of 1m) (Figure 6b), model 3 - asymmetric pile head defect (elimination of specific finite elements in the length of 1m) (Figure 6c), model 4 - asymmetric reduction of cross-section in the middle of the pile length (elimination of specific finite elements) (Figure 6d), model 5 - asymmetric reduction of cross-section in two locations along the pile length (elimination of specific finite elements) (Figure 6e), model 6 - significantly degraded pile along its full length (elimination of specific finite elements) (Figure 6f), model 7 - different elastic modulus in the pile-toe zone (changing the elastic modulus in the length of 2m) (Figure 6g) and model 8 - different elastic modulus and asymmetric reduction of cross-section at two locations along the pile (changing the elastic modulus and eliminating specific finite elements) (Figure 6h).

Table 1. Parameters of numerical pile models.

model	nodes	solid FE	no. of system equilibrium equations	degrees of freedom of the system masses
1	24381	19200	87786	73143
2	24131	18784	87036	71955
3	23621	18348	84954	70551
4	22963	17891	82263	68880
5	21095	15032	77928	60009
6	20991	14141	77616	59193
7	24381	19200	87786	73143
8	21095	15032	77928	60009

Table 1 shows the parameters of the numerical pile models. The appropriate wave-propagation time $t=8.3\text{ms}$ and the appropriate pile length $L=15.4\text{m}$ for the pile without discontinuities and defects (model 1) were identified using the finite-element method. The upper part of Figure 7 shows a reflectogram of the 3D solid pile model without a discontinuity (model 1) from the numerical analysis, while the lower part of Figure 7 shows the corresponding analytical solution obtained from Equation (6). There is a remarkable agreement for the wave-propagation times through the pile in both applied methods. In addition to the reflectogram-based considerations regarding the pile responses, the Fourier amplitude spectrum (FAS) was also applied. After the pile responses were considered based on the use of reflectograms at 12 measuring locations, the same was carried out along the 12 independent reflectograms for each pile model. These reflectograms were subsequently integrated into a single response using the reflectogram surfaces originally introduced in this study. The reflectograms were first considered in a 2D plane coordinate system and then transformed into a 2D polar coordinate system, while their final form was reached by transforming them into a 3D cylindrical coordinate system. The angle increment in the cylindrical coordinates is $\Delta\theta=30^\circ$. The location of the pile defect and the corresponding reduction in the modulus of elasticity were identified, among the others, on the basis of the differences in the velocity of the reflectogram of the damaged $v(t)_d$ and the healthy pile $v(t)_0$.

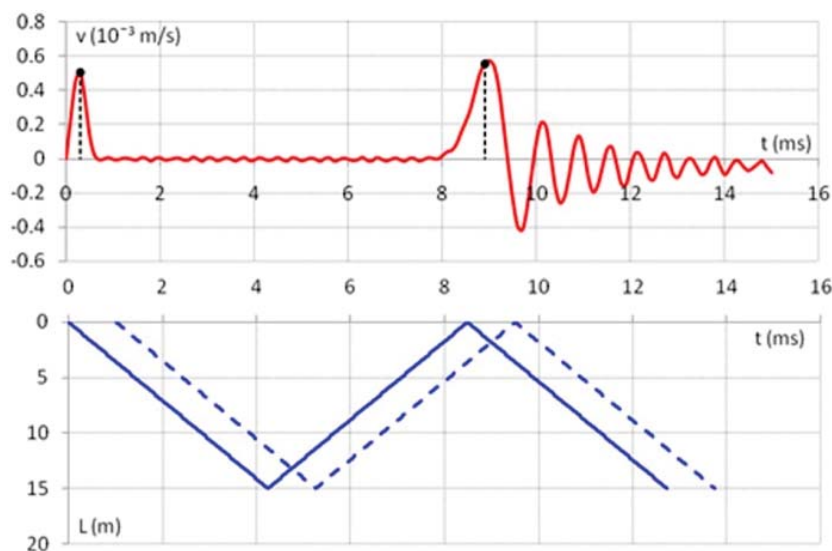


Figure 7. Reflectogram of the 3D solid pile model without discontinuities (model 1) and the corresponding analytical solution.

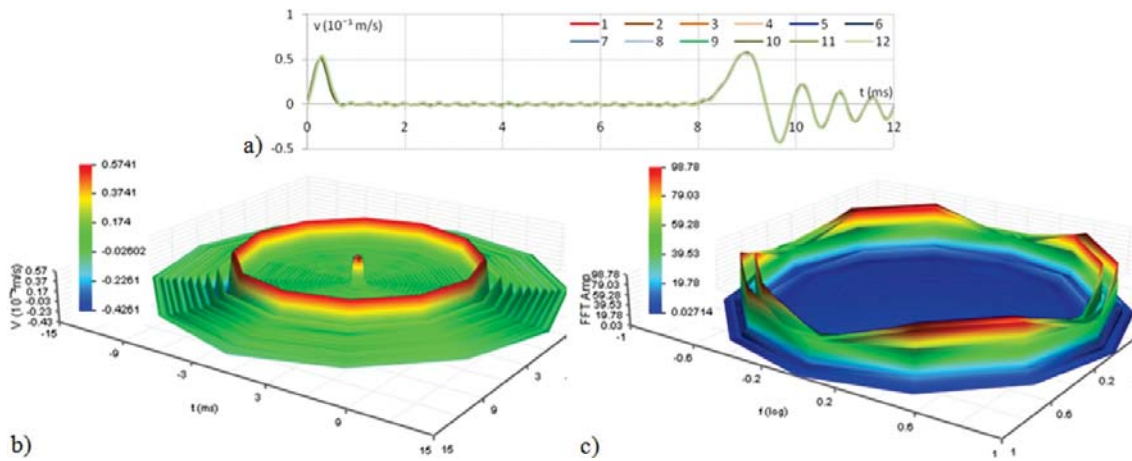


Figure 8. Numerical model of pile 1 - without discontinuities and defects: a) reflectograms, b) the 3D reflectogram surface, c) the 3D FAS spectrum surface.

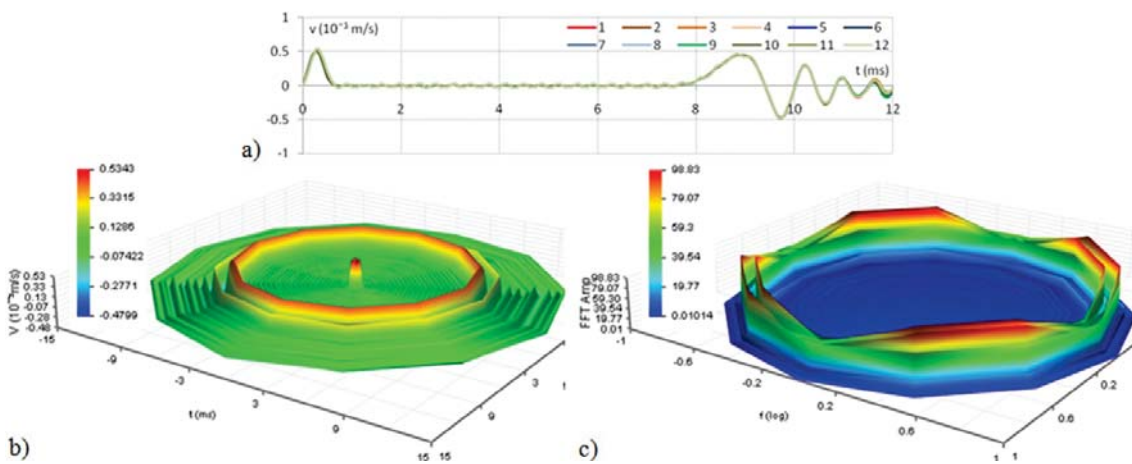


Figure 9. Numerical model of pile 2 - asymmetric pile-toe defect: a) reflectograms, b) the 3D reflectogram surface, c) the 3D FAS spectrum surface.

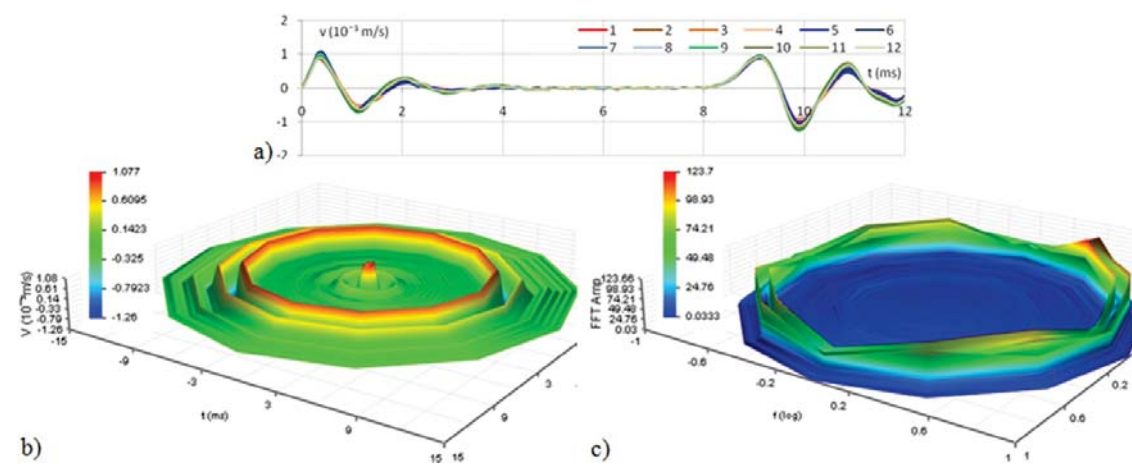


Figure 10. Numerical model of pile 3 - asymmetric pile-head defect: a) reflectograms, b) the 3D reflectogram surface, c) the 3D FAS spectrum surface.

Figures 8 to 15 show the reflectograms, the 3D reflectogram surfaces and the 3D surfaces of the FAS response spectrum for all eight pile models under consideration. All the reflectograms achieved in model 1 are identical, since the pile is without any discontinuities and defects, so that the reflectogram surface is an ideal rotationally symmetric surface (Figure 8). Almost identical reflectograms were also achieved in model 2, given the minimum asymmetry defect of the pile toe (Figure 9). On the other hand, since the pile toe defect was simulated based on the reduction of solid finite elements along the pile mantle near the toe, the central part of the pile remained intact, so that the waves were propagating and reflecting with minimum reduction, making the model 2 reflectograms similar to the model 1 reflectograms, except for the reduced wave-propagation velocity in the pile-toe zone. In model 3 with the asymmetric pile-head

defect, the wave propagation through the pile head was identified using a reflectogram based on the response rate shifting from a negative to a positive value (Figure 10). The length at which the reflectogram located the defect is $l=0.5v(t_1-t_0)=1.1\text{m}$, obtained from Equation (6), while the modelled defect length is 1m, while the level of agreement between the simulated PIT results and the numerical model results is obviously satisfactory. The length obtained based on the model 4 reflectogram with the asymmetric reduction of the cross-section in the middle of the pile length is $l=0.5v(t_2-t_1)=1.3\text{m}$, which corresponds to the length of the simulated discontinuity zone (Figure 11). In this model, the initiation and termination of the discontinuity zone are accompanied by shifting the velocity value in the middle of the pile length from positive to negative. The positive velocity value corresponds to the initiation of a discontinuity

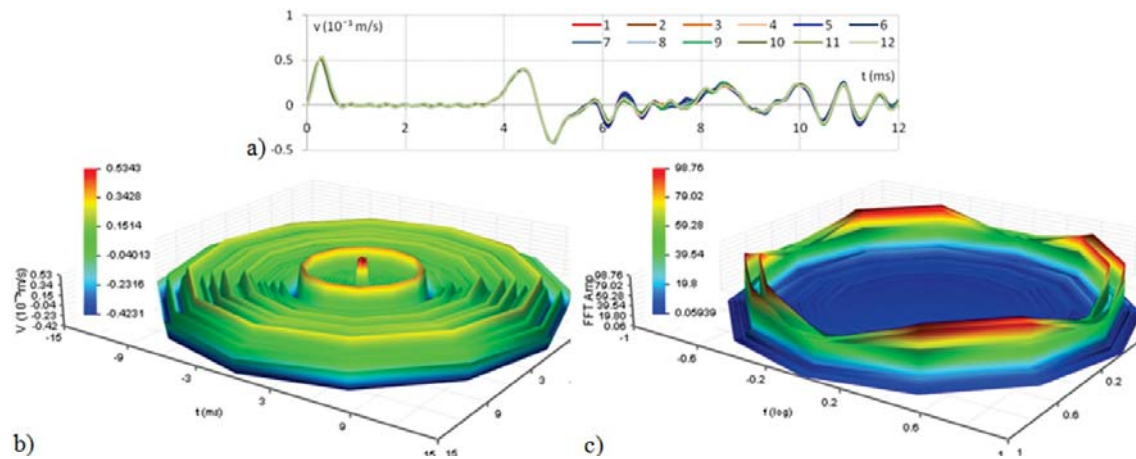


Figure 11. Numerical model of pile 4 - asymmetric reduction of cross-section in the middle of the pile length: a) reflectograms, b) the 3D reflectogram surface, c) the 3D FAS spectrum surface.

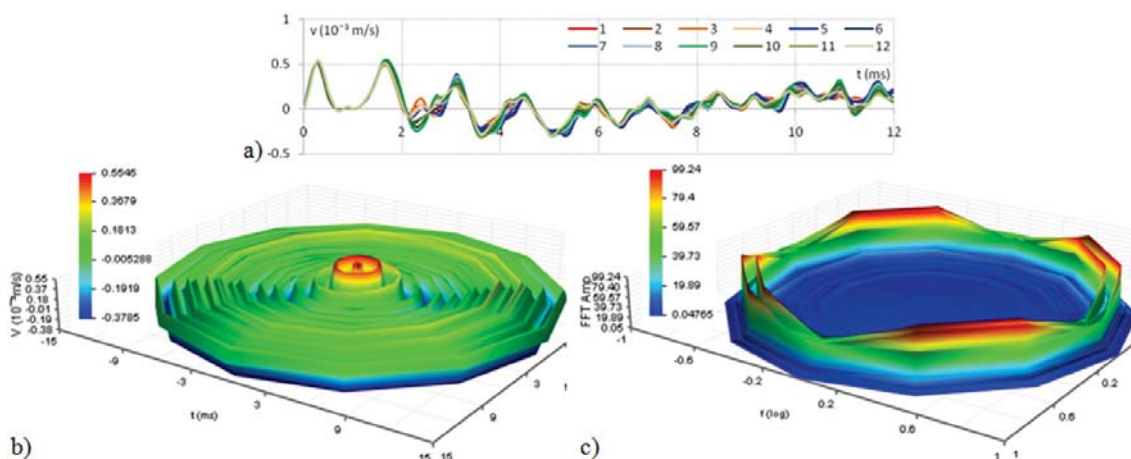


Figure 12. Numerical model of pile 5 - asymmetric reduction of cross-section in two locations along the pile length: a) reflectograms, b) the 3D reflectogram surface, c) the 3D FAS spectrum surface-

zone, while the negative velocity value corresponds to the termination of the discontinuity zone. In model 5 with an asymmetric reduction of the cross-section in two locations along the pile length the reflectogram identified the first discontinuity (Figure 12) as follows $l=0.5v(t_2-t_1)=2.4\text{m}$, while the length of the second discontinuity is $l=0.5v(t_4-t_3)=1.5\text{m}$. The reflectograms of this pile model are not all identical, due to the asymmetric and uneven discontinuities and defects, making the larger number of velocity shifts from the positive to the negative values obvious. There is an additional velocity shift on the transition between the two pile discontinuities, which is a consequence of the substantial irregularity of the discontinuities, as also evidenced by the reflectogram response for the diagonal measuring locations. The reflectograms obtained for the model 6 pile (with a significant

degradation along the full pile length) vary significantly, depending on the position of the measuring location (Figure 13). The defects in this pile were modelled based on the principle of the stochastic modelling of defects in the concrete, resulting in frequent changes of velocity on the reflectogram. In the case when the actual pile model results in this type of reflectogram, further pile strengthening is recommended or the pile needs to be replaced due to reduced capacity, stability, usability and durability. The model 7 is characterized by a different elastic modulus in the pile-toe zone, where the wave-propagation velocity is $v=2635.23\text{m/s}$ (Figure 14). This velocity is typical of poor-quality concretes; it is also typical for piles significantly degraded in the toe zone. The reflectogram is featured by the reduced wave velocity in the pile, which is a direct consequence of the different elastic modulus

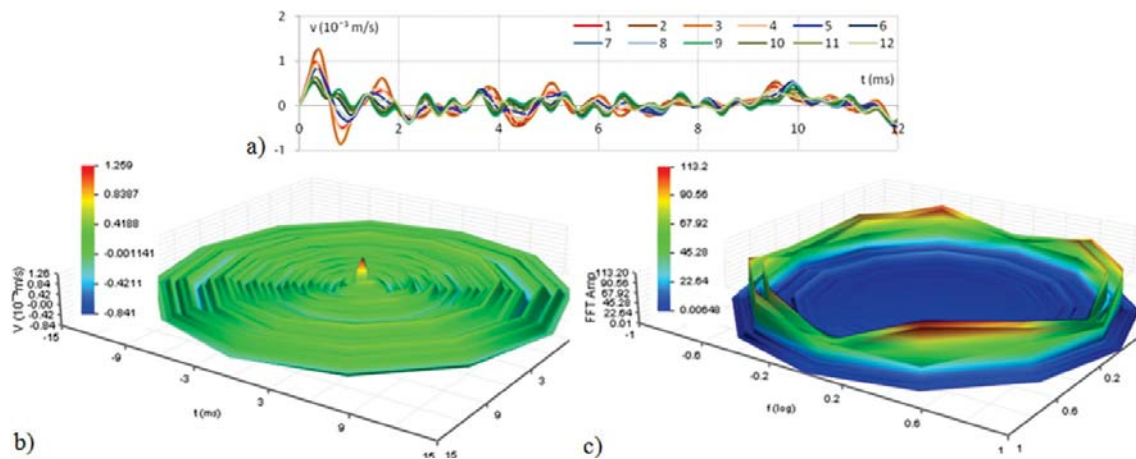


Figure 13. Numerical model of pile 6 - significant degradation along the full pile length: a) reflectograms, b) the 3D reflectogram surface, c) the 3D FAS spectrum surface.

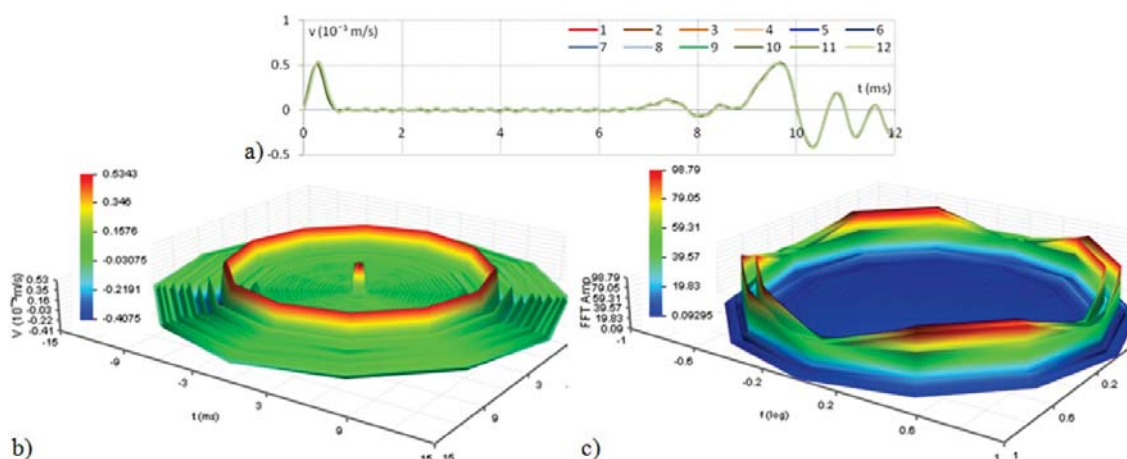


Figure 14. Numerical model of pile 7 - different elastic modulus in the pile toe zone: a) reflectograms, b) the 3D reflectogram surface, c) the 3D FAS spectrum surface.

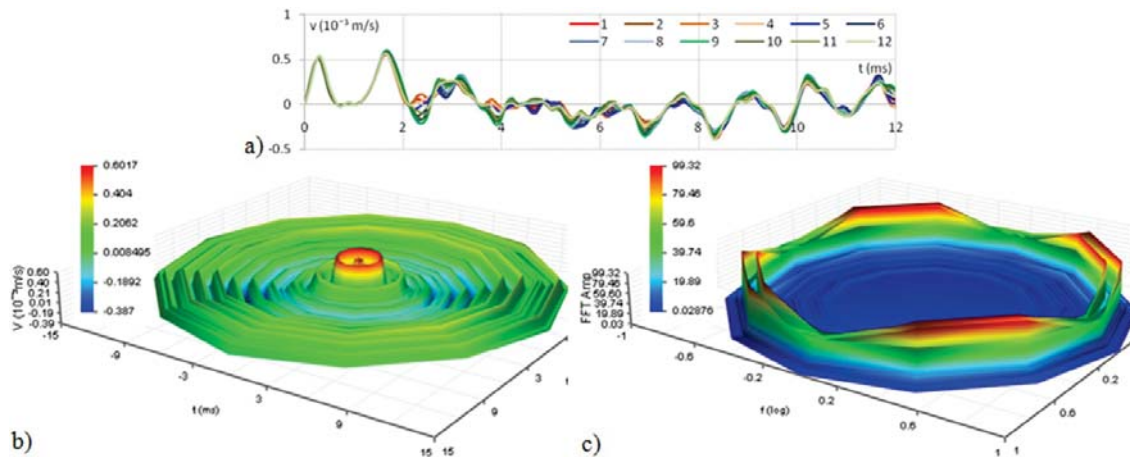


Figure 15. Numerical model of pile 8 - different elastic modulus and asymmetric reduction of cross-section in two locations along the pile length: a) reflectograms, b) the 3D reflectogram surface, c) the 3D FAS spectrum surface.

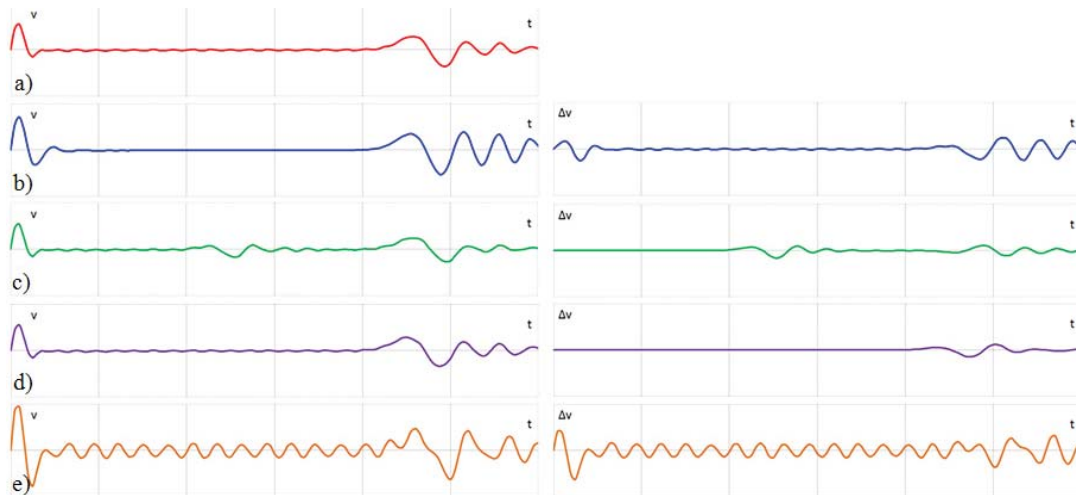


Figure 16. Reflectogram (left) and reflectograms obtained as the velocity difference Δv between the damaged $v(t)_d$ and the healthy pile $v(t)_0$ (right): a) no discontinuities and defects, b) pile-head defect, c) defect or reduced modulus of elasticity in the middle of the pile length, d) pile-base defect or reduced modulus of elasticity in the pile base zone, e) reduced modulus of elasticity in the pile head zone.

at this location. The zone of the reduction of the elastic modulus is initiated between lengths of 12.9 and 15m, where the reflectogram contains a change in the sign of the velocity. In model 8 with different elastic modulus and an asymmetric reduction of the cross-section in two locations along the pile length, there is a significant difference in the system response presented by the reflectograms (Figure 15). In the first part, up to the initiation of the reduction of the cross-section, the reflectograms are all identical, but along with the propagation of waves through the zone of discontinuity the nature of the response at the measuring locations is stochastic.

The typology of the reflectograms was conducted in order to facilitate the identification of the pile damage. Figure 16 shows the general reflectogram models (left) and the reflectograms obtained as the velocity differences Δv between the damaged $v(t)_d$ and healthy pile $v(t)_0$ (right): without discontinuities and defects (Figure 16a), pile-head defect (Figure 16b), defect or reduced modulus of elasticity in the middle of the pile length (Figure 16c), pile-base defect or reduced modulus of elasticity in the pile-base zone (Figure 16d), and reduced modulus of elasticity in the pile-head zone (Figure 16e).

7 SUMMARY AND CONCLUSIONS

This paper describes the development of discrete numerical 2D and 3D solid pile models with a discontinuity and defects to simulate the non-destructive testing using the pile integrity test (PIT). The pile discontinuity and defects were modelled by reducing the specific finite elements and using the staged degradation analysis (SDA). The effect of the degradation of the pile concrete quality is introduced through the reduction of the elastic modulus in specific zones. The wave-propagation response of the pile was analyzed based on a step-by-step numerical integration using the Hilber-Hughes-Taylor (HHT) method in the time domain. The concept of the system response analysis was originally formulated based on the integration of individual reflectograms into a reflectogram surface, which is generated in a 3D cylindrical coordinate system.

In addition to the pile without discontinuities and defects, seven different models of pile discontinuities and defects were considered: asymmetric pile toe, asymmetric pile-head defect, asymmetric reduction of cross-section in the middle of the pile length, asymmetric reduction of cross-section in two locations along the pile length, significantly degraded pile along its full length, different elastic modulus in the pile-toe zone and different elastic modulus and asymmetric reduction of the cross-section in two locations along the pile. Shifting in the response velocity on the reflectogram from positive to negative values indicates the locations of discontinuities and defects in the discrete 3D pile model, where there is a clear difference between the reflectograms depending on the position of the measuring locations.

The study defines the typological reflectogram models: without discontinuities and defects, pile-head defect, defect in the middle of the pile length or a reduced modulus of elasticity in the middle of the pile length, pile-base defect or a reduced modulus of elasticity in the pile-base zone, and a reduced modulus of elasticity in the pile-head zone. The identification of cracks in the pile is the next step in studying numerical simulations of the PIT.

ACKNOWLEDGEMENT

The research described in this paper was financially supported by the Ministry of Education and Sciences Republic of Serbia within the Project TR 36043. This support is gratefully acknowledged.

REFERENCES

- [1] Štrukelj, A., Pšunder, M., Vrecl-Kojc, H., Trauner, L. (2009). Prediction of the pile behaviour under dynamic loading using embedded strain sensor technology. *Acta Geotechnica Slovenica* 6, 65-77.
- [2] Trauner, L. (2012). The current state and trends in geotechnics. The 2nd International Scientific Meeting GTZ 2012, Tuzla, Bosnia and Herzegovina, 41-59.
- [3] Ding, X., Liu, H., Liu, J., Chen, Y. (2011). Wave propagation in a pipe pile for low-strain integrity testing. *Journal for Engineering Mechanics* 137, 9, 598-609.
- [4] Niederleithinger, E. (2006). Numerical simulation of non-destructive foundation pile tests. The 9th European Conference on NDT, Berlin, Germany.
- [5] Niederleithinger, E. (2008). Numerical simulation of low strain dynamic pile test. The 8th International Conference on the Application of Stress Wave Theory to Piles, Lisbon, Portugal, 315-320.
- [6] Zhang, C., Yang, S., Zhang, J., Xiao, N. (2010). The numerical simulation for the low strain dynamic integrity testing and its application in quality diagnosis of foundation pile. *Journal of Xiamen University (Natural Science)*, Xiamen, China.
- [7] Warrington, D., Wynn, R. (2000). Comparison of numerical methods to closed form solution for wave equation analysis of piling, The 13th Annual Meeting of the Tennessee Section of the American Society of Civil Engineers, Smyrna, USA.
- [8] Holeyman, A. (1992). Technology of pile dynamic testing, in: F. Barends (ed.), *Application of Stress-Wave Theory to Piles*, Balkema, 195-215.
- [9] Ambrosini, D., Ezeberry, J. (2005). Long piles integrity trough impact echo technique. *Mechanica Computational*, Buenos Aires, Argentina, 651-669.
- [10] Middendorp, P. (2005). Method statement sonic integrity testing (pile integrity testing). *Profound*.
- [11] Thilakasiri, H. (2006). Interpretation of pile integrity test (PIT) results. *Annual Transactions of IESL*, 78-84.
- [12] Likins, G., Rausche, F. (2000). Recent advances and proper use of PDI low strain pile integrity testing, in: Niyama and Beim (eds.), *Application of Stress-Wave Theory to Piles*, Balkema, 211-218.
- [13] Rorabugh, C. (2011). Notes on digital signal processing - practical recipes for design. *Analysis and Implementation*, Prentice Hall, New York, USA.
- [14] Liao, S., Roesset, J. (1997). Dynamic response of intact piles to impulse loads. *International Journal for Numerical and Analytical Methods in Geomechanics* 21,4, 255-275.

- [15] Hilber, H., Hughes, T., Taylor, R. (1977). Improved numerical dissipation for time integration algorithms in structural dynamics. *Earthquake Engineering and Structural Dynamics* 5, 3, 283-292.
- [16] Kim, D., Kim, H., Kim, W. (2002). Parametric study on the impact-echo method using mock-up shafts. *NDT&E International* 35, 8, 595-608.
- [17] SAP 2000, (2010). *Integrated Software for Structural Analysis and Design*, CSI Berkeley, USA.